Probe Design & Construction

F. David Doty
Doty Scientific Inc., Columbia, SC, USA

1 INTRODUCTION

From the early days of NMR, the word probe (or probehead) has been used to refer to the complete piece of equipment intimately associated with the sample (except the sample tube). For the simplest experiments, the probe consists of the mechanical structure required to hold the sample in the 'sweet spot' of the magnet, a coil surrounding the sample, a tuning capacitor, and an rf transmission line. However, most chemical problems of interest require control over the sample environment (temperature, electromagnetic irradiation, pressure, orientation, and re-orientation), and apparatus associated therewith becomes a part of the NMR probe.

The modern NMR probe is a complex piece of apparatus designed to accommodate all of the environmental requirements of the NMR experiment. The radiofrequency (rf) portion often includes (a) an rf 'observe' channel optimized for highest signal-to-noise-ratio (SNR, or S/N, also called sensitivity) at the X nucleus frequency, (b) a less efficient rf channel for heteronuclear decoupling (usually ^{1}H, except for indirect detection), and (c) another low-efficiency channel for magnetic field lock (usually ^{2}H). Variable temperature (VT) control is achieved with a resistive heater in a gas stream that flows over the sample. In high-resolution liquids probes, slow sample spinning (10–200 revolutions per second, Hz) about the $\boldsymbol{B}_0$ axis to average out azimuthal inhomogeneity in $\boldsymbol{B}_0$ is usually accomplished with a pneumatic system external to the probe, but high-speed sample spinning apparatus (200–26 000 Hz) for solids averaging techniques is an integral part of a solids probe.

One of the most demanding technical aspects of liquids probes is the requirement of extremely high $\boldsymbol{B}_0$ field homogeneity (as high as several parts per billion), but sometimes it is advantageous to be able deliberately to spoil the field homogeneity over precise time periods by applying field gradients.

For References see p. 3761

When very high gradients and fast switching are required, as in diffusion measurements or solids microscopy magnetic resonance imaging (MRI), the gradient coils must be as small as possible and incorporated into the probe. However, for most MRI work with samples larger than 40 mm, the gradient coils are external to the probe.

Another challenging technical requirement is often that of minimizing NMR background signals from construction materials that contain trace amounts of the nuclide of interest—particularly for highly sensitive proton (^{1}H) experiments. Other technical complications may stem from provisions for optical or microwave irradiation and operation at extreme temperatures.

Addressing the often conflicting requirements of high sensitivity, high resolution, large spectral bandwidth, low background signals, wide VT range, high-speed sample spinning, intense irradiation, and uniform field gradients requires careful attention to a number of problems in materials science, physics, electrical engineering, and mechanical engineering. The engineering effort often makes the price of a probe comparable to the price of a new sports car.

2 GENERAL CLASSES OF NMR PROBES

2.1 Liquids Probes

Approximately 80% of NMR experiments are performed on high-resolution liquids probes designed for samples in axially aligned glass tubes in superconducting magnets using saddle-shaped rf coils or slotted resonators for signal reception. They are often required to achieve a spectral resolution of several parts per billion on slowly spinning samples. A small fraction of their usage has been for in vivo experiments on small living animals or ex vivo or in vitro experiments on surgically removed tissues kept alive for short periods of time by perfusion with nutrients in saline solutions furnished by a flow system in the probe. Most multinuclear liquids probes have provided proton decoupling with multinuclear observe and deuterium lock, but recently many have been designed for inverse experiments (proton detection with *X*-nucleus decoupling). At present, high-resolution liquids probes are commercially available for experiments from $-180\,^{\circ}$C to $380\,^{\circ}$C.

2.2 Gradient Probes

Pulsed field gradient (PFG) and microscopy MRI probes are usually similar to conventional liquids probes with the addition of gradient coils for one or three axes respectively. PFG probes are used for the measurement of diffusion coefficients, solvent suppression, or selection of specific coherences. Their usage has grown very rapidly in the past several years because of the time savings they provide in two-dimensional NMR. Microscopy in vivo probes may include surface coils for improved localized signal reception.

2.3 Solids Probes

The original (and simplest) probe for NMR of solid samples is the wideline probe, which is normally characterized as being able to generate 90° pulse lengths less than 3 μs (spectral excitation bandwidths greater than 80 kHz) by withstanding peak rf coil voltages in excess of 3 kV. Often they are double tuned (DT) to permit cross polarization (CP) with high-power decoupling for increased sensitivity and resolution. High-speed magic angle spinning (MAS) of the sample is added in the CP MAS probe for line narrowing of spin-$\frac{1}{2}$ nuclei, and dynamic angle spinning (DAS) and double rotation (DOR) may be provided for quadrupolar nuclei. When sufficiently large single crystals of the sample can be grown, high-resolution spectra and the chemical shift tensor can be obtained using a single crystal probe that includes a suitable goniometer and crystal orientation mechanism.

3 HISTORICAL PERSPECTIVE ON NMR PROBES

Through the late 1960s 'NMR' implied 'proton NMR of liquids' unless specifically stated otherwise, and multinuclear probes were unheard of. There was a rather widespread misconception that sensitivity increased linearly with coil inductance, even though the early classic treatments[1,2] were sound. High-inductance solenoids (1–50 μH, compared with 40–200 nH for modern probes) wound around the sample tube could be used for efficient reception in the transverse field of the electromagnet, but audio field-modulation coils were needed to shift the detection frequency above the $1/\nu$ noise region of the phase-sensitive video detector. The orthogonal Helmholtz transmit coils could be driven with low-power (milliwatt) oscillators for most continuous wave (CW) techniques, and the transmit/receive coils were carefully isolated using Faraday shields and tuning paddles. Since low-impedance preamplifiers with low noise figures were not available, it was best to include the first stage of the preamplifier in the probe and match it (usually 300–2000 Ω) directly to the receive coil.

Although many time domain pulsed NMR experiments were performed in the first two decades of NMR for relaxation studies, the explosion of NMR techniques awaited the application of Fourier transform (FT) by Richard Ernst in 1966 to the time domain data to obtain the complete frequency domain spectra in a single free induction decay (FID). The increase in sensitivity was comparable to the ratio of the total spectral width to the narrowest line in the spectrum—often two or three orders of magnitude.[3,4] (See also ***Fourier Transform Spectroscopy***.)

Field shimming (homogenizing) was extremely crude and tedious prior to Golay's development of the theory and practice of orthogonal shim coils.[5] With the advent of FT NMR came more incentive to obtain higher resolution because of its dramatic impact on sensitivity. Ultrahigh purity (99.9995%) copper receive coils with precision magnetic compensation and Varian's sample spinner mounted on top of the probe quickly became standard. An external lock employing a sealed sample and separate coil (usually tuned to ^{19}F or ^{2}H) beside the sample coil was used to stabilize the field.[6]

The probe rf circuitry was also quickly impacted by FT NMR. To excite the entire spectral width with large Helmholtz coils at 60 MHz required 10–100 W and generated several kV across the coil, so impedance matching to the transmit circuit became important. The increase in sensitivity from FT NMR opened up the field of multinuclear MR—especially ^{13}C and ^{31}P.[7] The advantages in resolution and sensitivity provided by proton decoupling required double resonance circuits, which

For list of General Abbreviations see end-papers

made it more difficult to use separate transmit/receive coils, and double-tuned single-coil circuits with transmit/receive duplexers began to appear.[8,9] It is fair to say that modern NMR probe technology was ushered in by David Hoult in 1976 with his transparent analysis of S/N based on the obscure concept of reciprocity.[10] Today, separate transmit/receive coils survive only in single resonance MRI where the high rf homogeneity afforded by a large transmit coil is beneficial and small surface coils are optimum for reception.

Probe technology has matured over the past two decades, and major advances in most probe specifications are not expected. Nonetheless, probe technology will retain its pivotal role in NMR progress because even small improvements can contribute a lot to total system performance.

4 RADIOFREQUENCY ENGINEERING—BASICS

Basic rf engineering has been treated in a number of elementary texts[11,12] and introductory review articles,[13,14] but the probe engineer also needs a working understanding of some of the more advanced concepts in electromagnetic field theory.[15,16] NMR signal reception is different from (and simpler than) antenna theory, in that antennas are designed to receive electromagnetic waves in the far-field limit whereas NMR probes are designed to sense magnetic fields in the near-field limit.[17] While the rf circuits in NMR probes can usually be approximated with simple circuits and analyses, the critical importance of the probe to the total spectrometer performance justifies a level of detailed field and efficiency analysis seldom encountered outside of NMR probes. A number of articles[10,18–25] and a textbook[26] have presented excellent treatments of general NMR probe design problems over the past two decades. A summary of basic NMR probe electronics follows.

4.1 Capacitance

Capacitance (farads) is defined as electric charge per volt (Q/V), and capacitive energy storage is equal to $CV^2/2$. Stray capacitance can often be estimated to sufficient accuracy from the expression for the parallel plate capacitor C_p of area A (m^2), separation distance d (m), and dielectric constant k_d,

$$C_p = \frac{k_d \varepsilon_0 A}{d} \tag{1}$$

or from the expression for the low-frequency capacitance of a coaxial capacitor[21] of length h, dielectric o.d. d_o, and dielectric i.d. d_i,

$$C_c = \frac{2\pi k_d \varepsilon_0 (h + d_o)}{\ln(d_o/d_i)} \tag{2}$$

where ε_0 is the permittivity of free space, 8.84 pF m^{-1}. Parallel capacitors add algebraically, ($C_T = C_1 + C_2 + \ldots$), while series capacitors add reciprocally ($C_T^{-1} = C_1^{-1} + C_2^{-1} + \ldots$).

4.2 Inductance

The simplest definition of inductance L (henrys) comes from Faraday's law of induction—the induced voltage divided by the rate of change in current di/dt. For inductance calculations, the most practical 'definition' follows from the energy equation

$$U = i_T^2 L/2 \tag{3}$$

where U is the total energy in the magnetic field (the integral of $B^2/2\mu\mu_0$ over all space) and i_T is the current *at the pair of terminals* generating the magnetic field $\boldsymbol{B}$. [We follow popular usage of denoting the magnetic flux density or induction field $\boldsymbol{B}$ (T) as the 'magnetic field' and $\boldsymbol{H} = \boldsymbol{B}/\mu\mu_0$ as the field intensity (A m^{-1}) where μ is the relative permeability of the material.] For all NMR probes, μ is always unity. The permeability of free space μ_0 equals $4\pi \times 10^{-7}$ H m^{-1}.

The inductance of the finite, multiturn, single layer rf solenoid of Figure 1 with a constant pitch, an integral number of turns, and a high surface coverage is given in nH, for dimensions in mm, by the following expression:

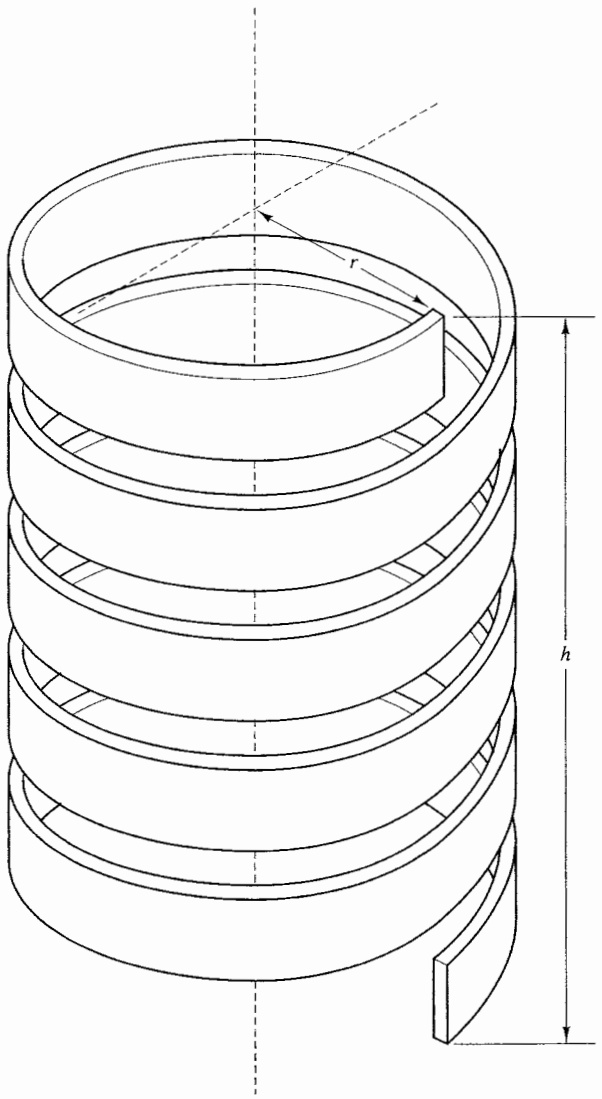

Figure 1 A five-turn solenoid

For References see p. 3761

$$L_S = \frac{4n^2r^2(1 - 0.2/n)}{h + 1.2r^{0.9}} \quad \text{[mixed]} \tag{4}$$

where n is the number of turns (Figure 1 has five turns), h is the *overall* axial length, and r is the effective inside radius, which for round wire is approximately equal to the inside coil radius plus 20% of the wire radius. The last term in the numerator corrects for the fact that the helix makes the effective coil length a little less than the overall length. The above expression is correct to within several per cent for $h/r > 0.2$. For the loop-gap resonator[27,28] (a single-turn solenoid, also called a split ring), the helix correction term is dropped, and the coefficient changes to 3.9 to correct for current concentrating at the ends of the ring. Higher order corrections for multiturn coils with low surface coverage can be added.

Lead (parasitic) inductance is usually best estimated by calculating the inductance of a loop-gap resonator having a length equal to the diameter of the lead wire and $r^2 = A_C/\pi$, where A_C is the area enclosed by the loop formed by the leads. Sometimes lead inductance is better estimated from the expression for the inductance L_C of a coaxial transmission line:

$$L_C = \frac{\mu_0 h}{2\pi} \ln\left(\frac{d_o}{d_i}\right) \tag{5}$$

Clearly from equation (5), series inductors add like resistors ($L_T = L_1 + L_2 + \ldots$); likewise, parallel inductors add reciprocally ($L_T^{-1} = L_1^{-1} + L_2^{-1} + \ldots$).

4.3 Single Resonance Circuits

4.3.1 Power

Figures 2 and 3 illustrate the basic *RLC* series and parallel circuits, respectively. The losses in the series *RLC* circuit of Figure 2 are best represented by the total effective series resistance R_s (from the coil, capacitor, leads, etc.). For the parallel circuit of Figure 3, the losses may be represented more conveniently by a total effective parallel resistor R_p. In both cases, the basic equations from ac circuits apply for rms power P and peak power P_P. (Power is assumed to be rms unless denoted otherwise.)

$$P = \frac{P_P}{2} = \frac{i_P^2 R_s}{2} = \frac{V_P^2}{2R_p} \tag{6}$$

Power ratios are often expressed in dB, $10\log(P_2/P_1)$, and power is often expressed in dBm—defined as dB relative to a milliwatt:

$$\text{dBm} \equiv 10\log(1000P) \tag{7}$$

In practice, peak-to-peak voltages ($2V_P$) are usually measured on an oscilloscope, and the measurements are significantly influenced by harmonic distortion, VSWR (Voltage Standing Wave Ratio), loading, and oscilloscope bandwidth. Most conventional liquids probes are excited with 100 W pulses of 10–80 μs at the observe frequency (usually the low frequency, LF) at duty cycles below 0.1% while they are driven with 10 W at the decouple frequency (usually ^{1}H, the high frequency, HF) at duty cycles below 50%. Solids probes typically see LF pulses of 200–400 W with duty cycles up to 1% while irradiating with HF power of 50–200 W at duty cycles below 30%. Whole body MRI probes are usually driven with 1–10 kW at duty cycles below 0.5%.

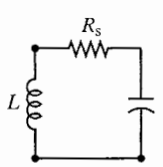

Figure 2 Series *RLC* circuit

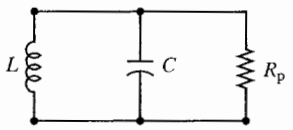

Figure 3 Parallel *RLC* circuit

4.3.2 Resonance

Since charge (q) equals CV and $i = dq/dt$, a capacitor reaches a steady-state (monochromatic) reactance X_C (analogous to resistance, V/i) of $1/i\omega C$ after several RC time-constants, where i is the imaginary unit, $\sqrt{-1}$. Likewise, since $V = -L\,di/dt$, an inductor has reactance $X_L = i\omega L$ and time constant L/R. For the normal high-Q condition ($Q = \omega_0/\Delta\omega_{\frac{1}{2}}$), resonance occurs when the inductive reactance X_L plus the capacitive reactance X_C equals zero. (Often the phase is omitted for convenience, but it must be remembered that the voltage phase in the inductor leads by 90° while in the capacitor it lags by 90° relative to that in the resistor.) Hence,

$$\omega_0 = \frac{1}{\sqrt{LC}} \tag{8}$$

At resonance, the series impedance of the series *RLC* circuit is R_s (since $X_L + X_C = 0$) and the parallel impedance of the parallel *RLC* circuit is R_p [since $(X_L X_C)/(X_L + X_C) = \infty$]. The 3 dB width $\Delta\omega_{1/2}$ of the resonance defines the quality factor of the unloaded (and unmatched) *RLC* circuit, and the following relationships are readily derived:

$$R_p = QX_L \tag{9}$$

$$R_s = X_L/Q = R_p/Q^2 \tag{10}$$

4.3.3 Matching

Since X_L is typically 20–200 Ω, R_s is usually less than 1 Ω and R_p is greater than 2000 Ω. For efficient coupling to the transmitter and preamplifier, the resonant circuit, transmission lines, preamplifier, and transmitter must all be matched to approximately the same impedance, although mismatches of up to a factor of two are often unimportant. The international standard is 50 Ω (except in the television industry, where it is 75 Ω). Figures 4 and 5 illustrate the two basic methods of impedance matching: shunt inductor and series capacitor.

The inductive matching technique has the advantage of not requiring a second high-voltage capacitor, but the matching

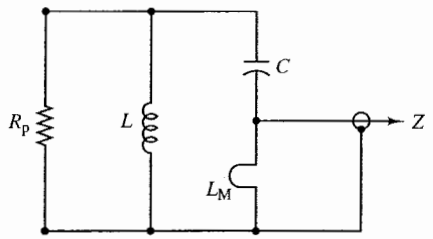

Figure 4 Shunt inductive matching circuit

range is limited by the difficulty of adjusting very small inductors. The required shunt inductor (for $R_p >> Z_0$) is

$$L_M = L_T\sqrt{Z_0/R_p} \tag{11}$$

where L_T is the total series inductance (L_s + L_M + leads) and Z_0 is the transmission line characteristic impedance—normally 50 Ω. The resonant frequency is calculated from L_T and C.

The capacitive matching circuit simplifies multinuclear (broadband) tuning requirements as high-voltage (HV) variable capacitors are readily available. The required match capacitance (again, for $R_p >> Z_0$) has reactance X_{CM} given by

$$X_{CM} = \sqrt{R_p Z_0} \tag{12}$$

and rms current equal to that in the transmission line, $\sqrt{P/Z_0}$. In practice, some combination of capacitive and inductive matching is often used, and capacitive voltage division is often employed to reduce the demands on the matching variable capacitor.[29] Properly 'pruned' transmission lines can also be used to transform impedance (see ***Probes for Special Purposes***).

5 SIGNAL-TO-NOISE RATIO AND B_1

5.1 Magnetization and the NMR Signal

The NMR voltage signal S from a sample with susceptibility χ, with nuclear spins precessing at angle ϕ in magnetic field $\boldsymbol{B}_0$ at angular frequency ω, detected by a coil that generates a circularly polarized (rotating) transverse field $\boldsymbol{B}_1(\boldsymbol{r})$, over the sample volume V_S for current i, may be shown from the principle of reciprocity[10,26] to be

$$S = \frac{\chi B_0 \omega}{\mu_0 i}\int_S \sin\phi\, B_1(\boldsymbol{r})\, dV \tag{13}$$

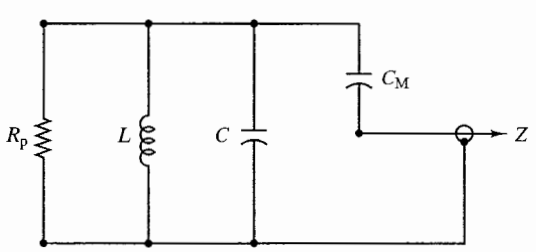

Figure 5 Series capacitive matching circuit

Simply put, the receiver coil need only be analyzed as a $\boldsymbol{B}_1$ transmitter. For a uniform $\boldsymbol{B}_1$ generated by a current i, immediately following a 90° pulse,

$$S = \frac{\chi B_0 \omega B_1 V_S}{\mu_0 i} \tag{14}$$

The equilibrium magnetization $\boldsymbol{M}_0$ is given by[1,6]

$$\boldsymbol{M}_0 = \frac{\chi \boldsymbol{B}_0}{\mu_0} = \frac{n_s \gamma^2 \hbar^2 I_x (I_x + 1)\boldsymbol{B}_0}{3k_B T_S} \tag{15}$$

where n_s is the number of spins at resonance per unit volume, γ is the magnetogyric ratio, I_x is the spin quantum number, k_B is Boltzmann's constant, T_S is the sample temperature, and $\hbar = h/2\pi$, where h is Planck's constant.

5.2 Thermal Noise

The Johnson (thermal) rms noise N from a resistor R_E for filter bandwidth $\Delta\nu$ (not ν/Q) is[1,2]

$$N = (4R_E k_B T_R \Delta\nu)^{1/2} \tag{16}$$

where T_R is the temperature of the resistor. (For R_E = 50 Ω, N = −168 dBm $Hz^{-1/2}$.) The effective series resistance (X_L/Q) of the loaded circuit is best determined by measuring Q. Other noise sources (interference, triboelectric, spurious, shot, microphonic, preamplifier) can usually be made negligibly small with careful engineering.[23]

5.3 B_1 in the Rotating Frame

A linearly polarized oscillating magnetic field $2B_1$ (as in a solenoid) may be decomposed into the sum of two oppositely rotating circularly polarized fields, each of magnitude B_1. One of these components can be used to drive NMR precession within a bandwidth approximately equal to its magnitude (in Hz) if it is transverse to $\boldsymbol{B}_0$; the other has no effect on NMR precession, as its frequency in the rotating frame is -2ω. From the Biot–Savart law,[15] B_1 at the center of a solenoid is given by

$$B_1 = \frac{\mu_0 n i}{2h\sqrt{1 + 4(r/h)^2}} \tag{17}$$

Using equations (3), (6), and (10), it may be shown that $U = PQ/\omega$, and B_1 may be expressed as follows for the infinite solenoid:

$$B_1 = \left[\frac{\mu_0 PQ}{2\omega V_C}\right]^{1/2} \tag{18}$$

where V_C is the coil volume. [Adding the term $1 + 4(r/h)^2$ in the denominator inside the brackets of equation (18) improves the accuracy for typical solenoids.]

The unloaded Q_0 of the typical multiturn solenoid (well below self-resonance and with high surface coverage) is, in mixed units, approximately

For References see p. 3761

$$Q_0 \approx 6\sqrt{hrf} \quad [\mathrm{MHz}^{1/2}\ \mathrm{mm}^{-1}] \tag{19}$$

Saddle coils (commonly, but incorrectly, called Helmholtz coils;[15] more properly they could be called Ginsberg[30] or Golay[5] coils) and slotted resonators[19,25] are better suited for liquids NMR in superconducting magnets, as they generate a transverse $\boldsymbol{B}_1$ while allowing axial access. Moreover, their axial symmetry makes it easier to obtain high $\boldsymbol{B}_0$ homogeneity. The coefficient in equation (19) is reduced to a value of 2 for saddle coils with medium surface coverage, as is necessary for orthogonal double resonance operation.

The loaded circuit quality factor Q_L will be lower than that of the coil because of losses in capacitors, shields, and sample. A convenient method of measuring Q_L is with a reflectance bridge, where the appropriate Δf value is measured at -7 dB return loss, which may be calibrated with a 21 Ω or 119 Ω load on a 50 Ω line.[23] (Q_L is not lowered much by 'matching' to the preamplifier if its noise figure is less than ~1 dB.)

For *any* coil, *average* B_1 in gauss over the usable volume may be expressed in mixed units by the following:

$$\langle B_1 \rangle = \beta \left[\frac{\eta_E P Q_L}{f V_C} \right]^{1/2} \quad [\text{mixed}] \tag{20}$$

where β is a dimensionless function of coil geometry, f is in MHz, V_C is in mL, and η_E is the rf efficiency—the fraction of the power delivered to the rf coil and sample.[21] The rf efficiency η_E is usually greater than 0.9 for single resonance circuits at low fields, but it may be less than 0.2 for double resonance at high fields. In practice, it is always necessary to measure rather than calculate Q_L, which then includes the capacitor losses. The above equation is still valid if η_E is then defined as $1 - \eta_L$, where η_L is the fraction of the power dissipated in inductors not generating B_1 (leads and coils added for multiple resonances).

For special high-resolution applications of solenoidal rf coils, the optimum h/r value is 2, and $\beta \approx 2.4$. For very lossy samples, the optimum h/r is the largest permitted by space constraints, and $\beta = \sqrt{10}$ for the infinite solenoid. For MAS, the optimum h/r is 3, and $\beta = 2.1$ when the coil is at the magic angle. For saddle coils and slotted resonators, β ranges from 0.8 to 1.4, depending on surface coverage, subtended angle, and the ratio of height to diameter.

A magnetic filling factor η_f may be defined by

$$\eta_f = \frac{\int B_1^2 \, dV}{\mu_0 U} \tag{21}$$

where the integration is over the sample volume V_S. From equations (3), (10), (20), and (21) comes a very practical (and exact) definition of the filling factor:

$$\eta_f = \frac{\beta^2}{20} \frac{V_S}{V_C} \tag{22}$$

5.4 S/N

From the above, the S/N from a single 90° pulse with an optimum filter [$1/(\pi\Delta\nu) = T_2$, the spin–spin relaxation time, and $\Delta\nu < \omega/2\pi Q_L$] can be written as follows:

$$\mathrm{S/N} = \frac{S}{2N} = \left[\frac{\hbar^2 \sqrt{\pi \mu_0}}{12 k_B^{3/2}} \right] \left[\frac{n_s \gamma I_x (I_x + 1) \sqrt{T_2}}{T_S \sqrt{T_R}} \right] (\eta_E \eta_f Q_L V_S)^{1/2} \omega^{3/2} \tag{23}$$

The extra factor of 2 in the denominator arises because S is the initial peak signal voltage that decays with time-constant T_2 and N is the rms noise voltage. The product of the two bracketed terms is 1.65×10^{-5} $\mathrm{s}^{3/2}$ $\mathrm{m}^{-3/2}$ for protons in water with $T_2 = 0.1$ s and $T_S = T_R = 300$ K.

A useful simplification of equation (23) is the following for given NMR conditions (sample, γ, $\boldsymbol{B}_0$, T_S, T_2, technique):

$$\mathrm{S/N} \propto \frac{V_S}{\tau_{90} \sqrt{P}} \tag{24}$$

where τ_{90} is the mean 90° pulse width obtained over sample volume V_S with power P.

5.5 Minimizing Losses

For small samples, the Q_L is usually dominated by coil resistance. However, above 400 MHz it may be dominated by capacitor losses unless extreme care is taken in their selection, and it may be necessary to parallel a number of low-value capacitors for sufficiently low capacitor losses. For large, lossy samples, Q_L and T_R are dominated by sample losses. Dielectric losses from electric fields in the sample may be reduced by decreasing the coil inductance and increasing the capacitance.[20,31] Usually, the only ways to reduce power P_S deposited by the inductive mechanism in a sample of uniform resistivity by a rotating $\boldsymbol{B}_1$ are to maximize the $\boldsymbol{B}_1$ homogeneity and to maximize the rms flux path length ξ for a given volume, but sometimes it is possible to use insulating films to suppress currents in the sample.[32] The presence of skin, fat, and bones in MRI can make the estimate of P_S as much as an order of magnitude too large when using a worst-case tissue resistivity ρ_S of 1.2 Ω m.

$$P_S \approx \frac{B_1^2 \omega^2 V_S^2}{16 \pi \rho_S \xi} \tag{25}$$

Equation (25) is equivalent to the low-frequency limit given by Carlson[24] for a sphere, but the inclusion of ξ improves loss predictions for nonspherical samples. The loaded Q_L may be estimated from the unloaded Q_0 and the sample Q_S:

$$Q_L = \frac{Q_0 Q_S}{(Q_0 + Q_S)} \tag{26}$$

For reasonably uniform, *linear* B_1, Q_S is approximately

$$Q_S \approx \frac{32 \pi \rho_S \xi V_C}{\mu_0 \eta_E \beta^2 \omega V_S^2} \tag{27}$$

The numerical coefficient in equation (27) is increased to 64 for circular polarization.

The ratio Q_0/Q_L has frequently been used as a figure-of-merit for coils in MRI, but this does not properly consider the dielectric losses nor the major effects of $\boldsymbol{B}_1$ inhomogeneity in surface coils.[33] Equation (24) provides a better figure-of-merit, but it still does not adequately evaluate homogeneity.

For list of General Abbreviations see end-papers

The 'birdcage' resonator of Edelstein et al. made quadrature coils practical for generating a single rotating $\boldsymbol{B}_1$.[22,34] Liquids and solids NMR find few applications for quadrature rf coils, as coil losses usually dominate. However, in MRI, when inductive sample losses dominate, quadrature coils offer up to a 40% improvement in S/N. For an advanced treatment of the birdcage resonator, the reader is referred to the article by Tropp.[35] (See also ***Birdcage & Other High Homogeneity Radiofrequency Coils for Whole Body Magnetic Resonance***.)

A proper calculation of L, B_1, and Q_0 requires a knowledge of the surface current distribution in the conductors—especially in single-turn resonators.[25] The so-called 'proximity effect' is ambiguous. A better method of determining current distribution in large conductors is to iterate on Biot–Savart integration, letting the currents move around in the conductors to a minimum inductance ($2U/i_T^2$) configuration. The current usually prefers to take the shorter paths (inside surface) and tends to concentrate near regions of high flux curvature (end edges) and high flux density (nearby shields). The normal component of the rf magnetic field always vanishes near the surface of conductors, and the current penetrates only to a depth given by the classical skin depth:

$$\delta = \left(\frac{2}{\omega\mu_0\sigma}\right)^{1/2} \tag{28}$$

where σ is the electrical conductivity. For copper at 300 K, δ = 6.4 μm at 100 MHz. Nonuniform surface current density is responsible for Q_0 being lower by a factor of 3–8 than would occur for uniform surface current density. In some cases, Q_0 may be improved by the use of Litz wire (woven wire, using individually enameled strands as fine as 0.03 mm).

6 DOUBLE RESONANCE

Two saddle coils, rotated 90° about the $\boldsymbol{B}_0$ axis provide a convenient method of doing double resonance NMR with good isolation. However, only the innermost coil can have the optimum filling factor, and sometimes it is beneficial to have the same spatial distribution of the two rf fields, $\boldsymbol{B}_1$ and $\boldsymbol{B}_2$. Also, triple- or quadruple-resonance NMR experiments are often useful. Thus, it is often desirable to double-tune or triple-tune a single sample coil, although Anderson described in 1973 a clever method of using three orthogonal, single-tuned coils.[36]

The number of modes in a resonant circuit will generally be equal to the number of unique inductors or capacitors, whichever is fewer. (Resonant transmission lines may count as either.) It is sometimes necessary to add additional inductors or capacitors (producing extraneous modes) to improve isolation or to achieve balance at the frequencies of interest, although this can complicate tuning.[37,38] The most common double-tuned circuit, shown in Figure 6, has been analyzed by several authors.[21,23,39] It has an HF parallel mode and an LF series mode. The efficiency at the HF is increased by *decreasing* L_S/L_H, where L_S is the sample coil inductance and L_H is the HF tuning coil inductance. On the other hand, efficiency at the LF is increased by *increasing* L_S/L_H. In principle, if the losses in L_H and the tuning capacitors can be made vanishingly small compared with sample losses, the efficiency can approach 100% at both frequencies.[40] Rise time, however, will be

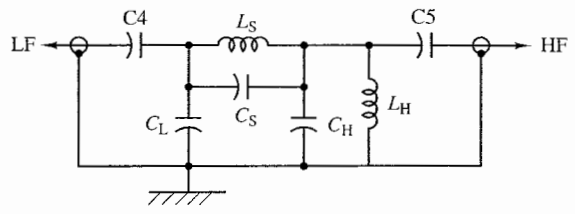

Figure 6 Double resonance circuit

degraded (because the total Q_L must increase), but this is seldom significant for in vivo experiments. For 8-mm sample coils, efficiencies at HF and LF are typically 40% and 75% respectively (when Q_L includes capacitor losses, as in the referenced analyses). From equations (20) and (23), B_1 and S/N are degraded only as the square root of the efficiency.

7 CONSTRUCTION MATERIALS AND TECHNIQUES

Although $\boldsymbol{B}_0$ homogeneity specifications sound frighteningly stringent, the capability of orthogonal shim systems is such that only in the immediate vicinity of the sample is magnetic susceptibility critical. Austenetic stainless steels (with SI volume susceptibility $\chi_V = \mu - 1 \approx 0.02$) can often be used for thin-walled Dewars surrounding the sample region and for Dewared transfer lines, although glass is preferred if space permits. It is, of course, desirable to minimize the amount of shimming effort required when the probe is changed, so low-susceptibility construction materials and thin sections are preferred. The magnetic susceptibilities of the components immediately above and below the sample region (in the B_z direction) are more significant, and axial and azimuthal symmetry are both important.[41,42]

The common aluminum alloys[43] 6063-T6 (0.7% Mg, 0.4% Si, up to 0.3% Fe) and 6061-T6 (1% Mg, 0.6% Si, 0.3% Cu, 0.3% Cr, up to 0.7% Fe) are usually acceptable for thin shield cylinders and support structure since the iron is usually in a nonmagnetic phase ($FeAl_3$ or Fe_2Al_7),[44] but they often present acoustic ringing problems below 15 MHz.[45] Jewelry bronze [copper alloy C22600, 87.5% Cu, 12.5% Zn, 0.005% (max.) Fe] is usually a better choice for shields and support structure because of its lower magnetism, much higher acoustic absorption, good electrical conductivity, high strength, and excellent finishing and joining properties. Iron content is also rather carefully controlled in the more readily available phosphor–tin bronzes, such as C51000 [94.8% Cu, 5% Sn, 0.2% P, 0.1% Fe (max.)]. Aluminum, silicon, and zinc bronzes (or brasses) have to be checked carefully if they are to be used within $r_b/3$ of the sample, where r_b is the bore radius, as iron contents can exceed 0.5%. Copper-rich iron compounds are not stable, and the solubility of iron in copper at 200 °C is only 13 ppm,[44] thus copper alloys are likely to be ferromagnetic unless the iron is bound up in iron-poor compounds (such as $FeAl_3$ or $FeSi_2$), in which case it is still strongly paramagnetic ($\chi_V \sim 2$ for Fe_2O_3). For B_0 above 2.16 T, the ferromagnetic components saturate with a high-field χ_V of $2.16\text{T}/B_0$.

The critical importance of high-integrity ground connections throughout multiple resonance probes cannot be overemphasized, especially as the wavelength becomes comparable to or

For References see p. 3761

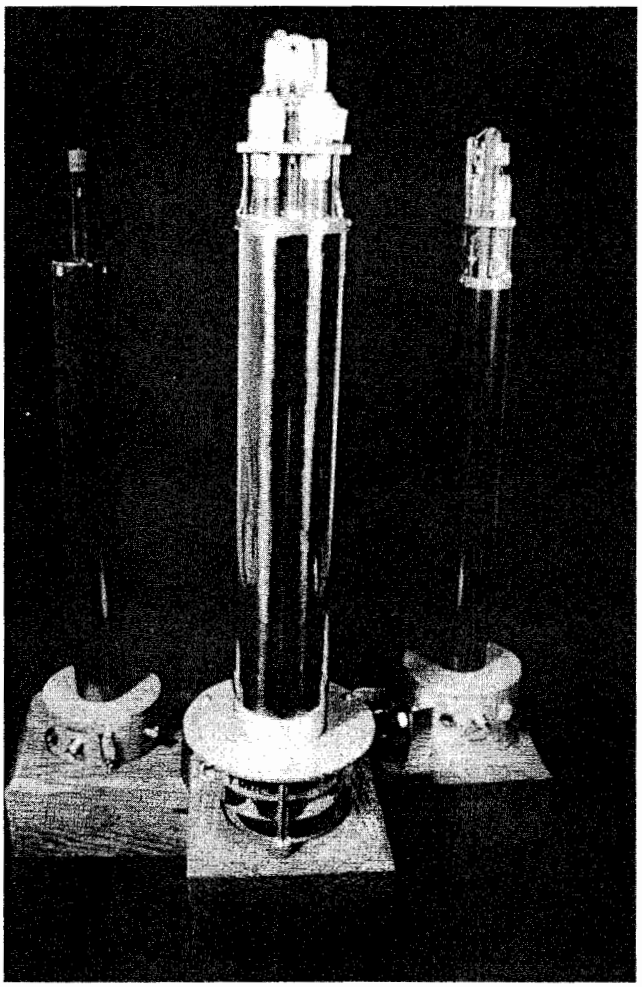

Figure 7 Three typical NMR probes

shorter than four times the maximum dimension of the electronics region. Welding, press-fits, and solder joints are preferred over silver-filled epoxy and silver paint.[23] The external shield cylinders are often anodized for an aesthetically pleasing finish that also helps eliminate variability in grounds. Figure 7 illustrates three typical NMR probes: a high-resolution liquids narrow bore probe, a CP MAS wide bore probe, and a single crystal probe with a goniometer.

Quartz is usually selected for coil forms in high-field magnets because of its lower dielectric loss, even though its magnetic, mechanical, and acoustic properties are inferior to those of Pyrex. Acoustic ringing in quartz, Macor, and ceramic capacitors may cause problems at frequencies up to 50 MHz. Zirconia has often been used in MAS probes for solids because of its superior mechanical properties.

One of the best engineering thermoplastics is polyether ketone (PEK) because of its low dielectric loss and excellent chemical, thermal, and dimensional stability at modest cost, but other insulating materials (Kel-f, Teflon, Macor, Vespel, zirconia) are often chosen for specific background or thermal considerations. Fiberglass reinforced composites are also widely used, but they must be cleaned well after machining to remove traces of steel from the tools, and the glass fibers may produce aluminum and silicon background signals. Excellent epoxies are available for securing components and mounting coils—such as Epo-Tek 354, 360, and 377 from Epoxy Technology, Inc., Billerica, MA, USA. Several brands of Kel-f and heat-shrink Teflon have sufficiently low hydrogenous content for critical proton applications, but experimentation and careful control are necessary.

8 THERMAL ENGINEERING

Linewidth and lineshape are often critically dependent on temperature control and stability.[46] Most commercial probes are intended to operate from −100 °C to +120 °C, but special liquids probes are commercially available for operation from −170 °C to +380 °C, and solids probes are available to cover the range 35–900 K. Temperatures are usually regulated by using a dc resistive heater (designed for minimal magnetic interaction) to heat a stream that is directed past the sample.

First-order heat-transfer calculations and simple power balance analysis are generally sufficient in the probe design. The heater power P_H required to increase the temperature of the gas by δT with specific heat C_p (1000 J kg^{-1} K^{-1} for N_2) and flow rate G (typically 1–2 g s^{-1} for MAS probes) is

$$P_H = GC_p\delta T \tag{29}$$

The gas temperature is usually measured with a copper–constantan thermocouple shortly before it reaches the sample, but optical sensors have also been used.[47] Platinum resistors (RTDs) are best in the range from 20–75 K and above 700 K, but in the intermediate range they are not as accurate as a thermocouple unless small magnetic-field-dependent corrections are made. They are often used to sense the heater temperature for protection in the event of inadvertent loss of gas flow. The control problems are more difficult than usually encountered elsewhere because of the requirement for precision temperature control of a stream of low specific heat that may encounter large fluctuations in flow rate. Standard PID (proportional-integral-derivative) control algorithms have been incorporated within the past several years by all manufacturers with vast improvements over the simple PI algorithms used previously. Dynamic control stability can be further improved by adding a power estimate that is a function of temperature and flow rate, and fuzzy logic may have advantages. Lead shot has occasionally been used for a thermal ballast because of its high volumetric specific heat and low Debye temperature (105 K).

Heat-transfer calculations are often limited to simple conduction calculations through thin sheets:

$$P_T = k_T A\delta T/d \tag{30}$$

where P_T is the thermal conduction power (W), k_T the thermal conductivity (W m^{-1}) of the material, A the area perpendicular to the direction of heat transfer, δT the temperature difference between the two surfaces, and d the thickness in the direction of heat transfer. The other common conduction problem is through a thick-walled tube with i.d. d_i, o.d. d_o, and length h:

$$P_T = \frac{2\pi k_T h\delta T}{\ln(d_o/d_i)} \tag{31}$$

The high Reynolds numbers (often greater than 10^5) that are seen in Dewared transfer lines result in a very high heat transfer through the bare glass or metal joints unless they are lined internally with plastic tubing, in which case the above equation can be used to estimate the losses.

The extreme temperatures that are often desired[48–50] can make differential thermal expansion responsible for stresses that exceed the rupture limit of one of the components in the probe if not properly designed. However, most of the materials used in NMR probes have high strength. The exceptions, Macor and glasses, tolerate high compressive stresses. Hence, even these materials can often be used with plastics in properly designed situations even though their thermal expansions differ widely. Macor is the only commonly used material that is likely to rupture from internal steady-state thermal stresses, as its maximum thermal stress temperature ($T_T = S/b_T E$, where S is tensile strength, b_T thermal expansion coefficient, and E the Young's modulus of elasticity) and thermal conductivity are both very low.

9 GRADIENT NMR PROBES

By applying magnetic field gradients in three orthogonal directions ($\delta B_z/\delta x$, $\delta B_z/\delta y$, $\delta B_z/\delta z$), it is possible to use NMR to image macroscopic structures, and indeed this has made clinical magnetic resonance imaging (MRI) an important medical diagnostic technique.[51,52] Obtaining spatial resolution below 1 mm on liquid-like samples requires gradients above the 10 m T m^{-1} available in most clinical MR machines. Higher gradients are easily obtained by reducing the size of the gradient coils or improving their efficiency. MR microscopy generally involves incorporating the gradient coils into wide-bore or narrow-bore probes along with small rf coils so that spatial resolution down to 10 μm can be obtained on liquid-like samples. Limited imaging experiments are also then possible on solid samples.[53]

Single axis gradients ($\delta B_z/\delta z$) based on Maxwell pairs (sometimes called anti-Helmholtz coils) are much easier to implement in small spaces and are very useful for diffusion experiments using pulsed field gradients (PFG).[54] Similar probes (with lower gradient coefficients, to keep digital-to-analog convertor and amplifier drift requirements more manageable) have recently become very popular for gradient enhanced spectroscopy (GES), as the run time is often dramatically reduced for 2D NMR.

Rapid switching of large gradient coils requires high-power audio amplifiers (up to 500 kW). Hence, the switching efficiency η_s is very important:

$$\eta_s = \frac{\alpha^2 d_S^4 h_S}{\mu_0 L} \tag{32}$$

where α is the gradient coefficient (T A^{-1} m^{-1}), d_S the sample diameter, h_S the sample length, and L the gradient coil inductance. (The gradient coefficient is sometimes called the 'efficiency', but the above dimensionless definition is more consistent with other efficiency definitions.) The 'fingerprint' design of Schenck et al.[55] achieves much higher η_s values than earlier Golay coils, but new proprietary designs achieve even higher efficiency.

Image linearity has often been described in terms of field linearity—the relative difference between the gradient field and a linear field at the edge of the sample. A better definition of image linearity is rms local deviation of the gradient from its mean value throughout the sample volume. This has also been called differential linearity. It is sometimes desirable to use highly nonlinear local gradients (more than 40% local deviation) and image distortion correction software so that higher gradients can be achieved,[56] but local deviation below 10% is usually preferred.

When the gradients are switched, eddy currents are induced in the cold radiation shield of the magnet that have long decay times because of the ultralow resistivity of copper below 40 K. Active shielding of the gradients greatly reduces the external fields generated by the gradients and permits rapid pulse techniques without excessive cryogen boiling or high-order compensation techniques.[57,58] Acoustic resonances in the gradient coils are then likely to limit gradient decay time, particularly at very high fields, but novel coil geometries are becoming available that greatly reduce this electromechanical or acoustic efficiency.

10 RELATED ARTICLES

Gradient Coil Systems; Instrumentation for the Home Builder; Probes for High Resolution; Radiofrequency Systems & Coils for MRI & MRS; Sensitivity of Whole Body MRI Experiments; Solid State Probe Design; Spectrometers: A General Overview; SQUIDs; Surface Coil NMR: Quantification with Inhomogeneous Radiofrequency Field Antennas.

11 REFERENCES

1. A. Abragam, 'The Principles of Nuclear Magnetism', Oxford University Press, Oxford, UK, 1961.
2. W. G. Clark, *Rev. Sci. Instrum.*, 1964, **35**, 316.
3. R. R. Ernst and W. A. Anderson, *Rev. Sci. Instrum.*, 1966, **37**, 93.
4. R. R. Ernst, in 'Advances in Magnetic Resonance', ed. J. S. Waugh, Academic Press, New York, 1966, Vol. 2, pp. 1–135.
5. M. J. E. Golay and N. J. Rumson, *US Pat. 3 569 823*, 1971.
6. H. D. W. Hill and R. E. Richards, *J. Phys. E, Ser. 2*, 1968, **1**, 977.
7. D. G. Gillies, in 'Nuclear Magnetic Resonance', ed. R. K. Harris, Chemical Society, London, 1972, Vol. 1, pp. 176–180.
8. J. D. Ellett, M. G. Gibby, U. Haeberlen, L. M. Huber, M. Mehring, A. Pines, and J. S. Waugh, in 'Advances in Magnetic Resonance', ed. J. S. Waugh, Academic Press, New York, 1971, Vol. 5, pp. 117–176.
9. D. D. Traficante, J. A. Simms, and M. Mulcay, *J. Magn. Reson.*, 1974, **15**, 484.
10. D. I. Hoult and R. E. Richards, *J. Magn. Reson.*, 1976, **24**, 71.
11. M. J. Wilson, 'The ARRL Handbook for the Radio Amateur', ARRL, Newington, CT, USA, 1987.
12. 'Basic Electronics', US Navy Bureau of Naval Personnel, Dover, NY, 1973.
13. R. E. Gordon, *Phys. Med. Biol.*, 1985, **30**, 8, 741.
14. D. D. Traficante, *Concepts Magn. Reson.*, 1989, **1**, 73.
15. J. R. Reitz and F. J. Milford, 'Foundations of Electromagnetic Theory', Addison-Wesley, Palo Alto, 1967.
16. J. D. Jackson, 'Classical Electrodynamics', 2nd edn., Wiley, New York, 1975.
17. D. I. Hoult, *Concepts Magn. Reson.*, 1989, **1**, 1.
18. D. I. Hoult, *Prog. NMR Spectrosc.*, 1978, **12**, 41.

19. H. J. Schneider and P. Dullenkopf, *Rev. Sci. Instrum.*, 1977, **48**, 68.
20. D. I. Hoult and P. Lauterbur, *J. Magn. Reson.*, 1979, **34**, 425.
21. F. D. Doty, R. R. Inners, and P. D. Ellis, *J. Magn. Reson.*, 1981, **43**, 399.
22. C. Hayes, W. Edelstein, J. Schenck, O. M. Mueller, and M. Eash, *J. Magn. Reson.*, 1985, **63**, 622.
23. F. D. Doty, T. J. Connick, X. Z. Ni, and M. N. Clingan, *J. Magn. Reson.*, 1988, **77**, 536.
24. J. W. Carlson, *J. Magn. Reson.*, 1988, **78**, 563.
25. G. J. Kost, S. E. Anderson, G. B. Matson, and C. B. Conboy, *J. Magn. Reson.*, 1989, **82**, 238. (Improved methods of treating non-uniform surface current distributions have recently been developed: S. Crozier, K. Luescher, L. K. Forbes, and D. M. Doddrell, *J. Magn. Reson., Ser. B*, 1995, **109**, 1.)
26. C.-N. Chen and D. I. Hoult, 'Biomedical Magnetic Resonance Technology', Adam Hilgar, New York, 1989.
27. W. N. Hardy and L. A. Whitehead, *Rev. Sci. Instrum.*, 1981, **52**, 213.
28. M. F. Koskinen and K. R. Metz, *J. Magn. Reson.*, 1992, **98**, 576.
29. F. D. Doty, *US Pat. 4 710 719*, 1987.
30. D. M. Ginsberg and M. J. Melchner, *Rev. Sci. Instrum.*, 1970, **41**, 122.
31. D. W. Alderman and D. M. Grant, *J. Magn. Reson.*, 1979, **36**, 447.
32. H. Kugel, *J. Magn. Reson.*, 1991, **91**, 179.
33. J. J. H. Ackerman, *Concepts Magn. Reson.*, 1990, **2**, 23.
34. W. A. Edelstein, J. F. Schenck, O. M. Mueller, and C. E. Hayes, *US Pat. 4 680 548*, 1987.
35. J. Tropp, *J. Magn. Reson.*, 1989, **82**, 51.
36. W. A. Anderson, *US Pat. 3 771 055*, 1973.
37. S. M. Holl, R. A. McKay, T. Gullion, and J. Schaefer, *J. Magn. Reson.*, 1990, **89**, 620.
38. F. D. Doty, *US Pat. 5 162 739*, 1992.
39. E. Najim and J.-P. Grivet, *J. Magn. Reson.*, 1991, **93**, 27.
40. J. R. Fitzsimmons, H. R. Brooker, and B. Beck, *Magn. Reson. Med.*, 1989, **10**, 302.
41. H. D. Hill and A. P. Zens, *US Pat. 4 517 516*, 1985.
42. H. D. Hill, *US Pat. 4 563 648*, 1986.
43. J. R. Davis (ed.), 'Metals Handbook', 10th edn., ASM International, New York, 1990, Vol. 2.
44. M. Hansen (ed.), 'Constitution of Binary Alloys', 2nd. edn., McGraw-Hill, New York, 1989.
45. M. L. Buess and G. L. Petersen, *Rev. Sci. Instrum.*, 1978, **49**, 1151.
46. A. Allerhand and S. R. Maple, *J. Magn. Reson.*, 1988, **76**, 375.
47. H. J. Williams, Y. Gao, A. I. Scott, M. H. Gross, and M. H. Sun, *J. Magn. Reson.*, 1988, **78**, 338.
48. F. D. Doty, J. B. Spitzmesser, and D. G. Wilson, *US Pat. 5 202 633*, 1993.
49. M. S. Conradi, *Concepts Magn. Reson.*, 1993, **5**, 243.
50. J. F. Stebbins, E. Schneider, J. B. Murdoch, A. Pines, and I. S. E. Carmichael, *Rev. Sci. Instrum.*, 1986, **57**, 39.
51. P. Mansfield and P. G. Morris, in 'Advances in Magnetic Resonance', ed. J. S. Waugh, Academic Press, New York, 1982, Vol. 12, Suppl. 2.
52. D. G. Taylor, R. Inamdar, and M.-C. Bushell, *Phys. Med. Biol.*, 1988, **33**, 6, 635.
53. D. G. Cory, J. W. M. van Os, and W. S. Veeman, *J. Magn. Reson.*, 1988, **76**, 543.
54. P. T. Callaghan and Y. Xia, *J. Magn. Reson.*, 1991, **91**, 326. (Important improvements in the original technique have recently been developed: D. Wu, A. Chen, and C. S. Johnson, *J. Magn. Reson., Ser. A*, 1995, **115**, 260.)
55. J. F. Schenck, M. A. Hussain, and W. A. Edelstein, *US Pat. 4 646 024*, 1987.
56. P. Roemer, *US Pat. 4 926 125*, 1990.
57. P. Mansfield and B. Chapman, *J. Magn. Reson.*, 1986, **66**, 573. (Force cancellation has recently been described: R. Bowtell and P. Mansfield, *Magn. Reson. Med.*, 1995, **34**, 494.)
58. J. J. Van Vaals and A. H. Bergman, *J. Magn. Reson.*, 1990, **90**, 52.

Biographical Sketch

F. David Doty. *b* 1950. B.A., Physics, 1972, Anderson University, IN, USA, Ph.D., 1983, Physics, University of South Carolina. Began work in NMR under Paul Ellis, 1979. President of Doty Scientific, Inc., 1982–present. Approx. 20 publications and 15 patents. Research interests include rf electronics, NMR probe technology, electromagnetism, manufacturing, turbomachinery, energy conversion cycles, ceramics engineering, acoustics, economics, and religions.

Probes for High Resolution

Howard D. W. Hill

Varian Associates, Palo Alto, CA, USA

1 INTRODUCTION

The NMR probe provides the coupling between the nuclear spins of the sample and the spectrometer electronics. As such, it must provide a rotating radiofrequency (rf) field perpendicular to the polarizing magnetic field to excite the spins and, similarly, detect the rotating magnetization of the spins. While these considerations apply to any NMR probe, a particularly important requirement for high-resolution NMR probes is to minimize the perturbation of the polarizing magnetic field so as to maintain the inherent resolution of the signals. This has become more important as the proton resonance frequency of high-resolution spectrometers has increased from the earliest values of 30 MHz to 750 MHz or more.

For a given magnetic field strength, the probe is a primary determinant in the *sensitivity* of a *spectrometer*. Sensitivity can be improved by using a larger sample, thereby including more spins, provided that the field homogeneity can be maintained

For list of General Abbreviations see end-papers